https://doi.org/10.1016/j.apacoust.2016.08.017

Sound attenuation of a periodic array of micro-perforated tube mufflers

Xiaofeng Shi and Cheuk-Ming Mak*

Department of Building Services Engineering, The Hong Kong Polytechnic University, Hung Hom, Kowloon, Hong Kong

*Corresponding author.
E-mail Address: cheuk-ming.mak@polyu.edu.hk (C.M. Mak).
Telephone: +852 2766 5856
Fax: +852 2765 7198

Abstract

The wave propagation in a periodic array of micro-perforated tube mufflers is investigated theoretically, numerically and experimentally. Because of the high acoustic resistance and low mass reactance due to the sub-millimeter perforation, the micro-perforated muffler can provide considerable sound attenuation of duct noise. Multiple mufflers are often used to enhance attenuation performance. When mufflers are distributed periodically in a duct, the periodic structure produces special dispersion characteristics in the overall sound transmission loss. The Bloch wave theory and the transfer matrix method are used to study the wave propagation in periodic micro-perforated tube mufflers and the dispersion characteristics of periodic micro-perforated mufflers are examined. The results predicted by the theory are compared with finite element method simulation and experimental results. The results indicate that the periodic structure can influence the performance of micro-perforated mufflers. With different periodic distances, the combination of the periodic structure and the micro-perforated tube muffler can contribute to the control of lower frequency noise with a broader frequency range or improvement of the peak transmission loss around the resonant frequency.

Keywords: Periodic structure, micro-perforated muffler, transmission loss

1. Introduction

A micro-perforated panel (MPP) is composed of a thin plate across whose surface are distributed holes of sub-millimetric size. Maa [1] initially proposed an approximate theory to predict the impedance of an MPP, which revealed that the panel itself can provide high acoustic resistance and low mass reactance, making the structure an efficient sound absorber. The MPP was introduced as an alternative to conventional porous absorbers avoiding the problems of bacterial contamination and small particle discharge. Many studies have since been conducted on the application of MPPs in fields such as room acoustics [2-7] and environmental noise control [8, 9]. MPP absorber arrays have been studied to improve the sound absorption performance. These studies have shown that the parallel arrangement of different MPP absorbers can result in broader absorption bandwidth compared to a single MPP absorber[10, 11].

In addition to its application in the field of room acoustics, the MPP has also been used to attenuate noise in duct systems [12, 13]. The micro-perforated tube muffler consists of micro-perforated tubes backed by air cavities. This kind of muffler is similar to conventional silencers except for its sub-millimeter perforation and the absence of porous material in the cavities. Because there is no fibrous material, the muffler can be used in situations where there are concerns about hygiene and health problems, such as hospitals and food industries. MPPs are usually made from metal or plastic and the cost for cutting the micro-perforated holes used to be high in the past. Nowadays the holes can be punched easily into metal or plastic panels and low cost

MPPs are available for commercial use[7, 14]. Liu et al. [15] applied the micro-perforated panel for duct noise control and compared the transmission loss of an MPP muffler with that of a muffler lined with foam. The results showed that the sound attenuation performance of the MPP was comparable to traditional sound absorbing materials with the same occupied volume in the muffler. Allam and Abom [16] also investigated mufflers based on the micro-perforated panel. Their findings revealed that the MPP muffler could provide a performance equivalent to a dissipative muffler with fiber material. Kabral et al. [17] experimentally studied MPP muffler with different configuration (different geometrical shapes of the apertures and the porosities of the micro-perforation). The MPP muffler was compared with the conventional muffler and the experiment results suggested that the MPP muffler could achieve the attenuation performance of the conventional muffler with porous materials. Although the MPP muffler is a little larger than the conventional muffler, the MPP muffler is lighter in the absence of the filled fibrous materials.

Although many studies have been carried out on the performance of perforated mufflers [18-20], the perforated screen is usually used to retain fibrous material and the perforation diameter of such mufflers is usually greater than a millimeter, unlike the micro-perforated tube mufflers. Wu [12] presented a preliminary study evaluating the sound attenuation of MPP silencers and discussed the effect of geometric parameters on silencer performance. Allam and Åbom [16] found that the micro-perforated muffler had minima at higher frequencies. These minima occurred due to the resonances in the outer chamber and were reduced by introducing an

uneven split to the outer chamber. Wang et al. [21] introduced micro perforation to a light plate silencer to broaden the effective frequency range of noise control. The vibration of the light micro-perforated plate was taken into account and the proposed hybrid plate silencer with micro-perforation provided wider stopbands than the plate silencer without micro-perforation. Previous studies used multiple MPP absorbers to achieve a broader frequency range for noise control and to attenuate duct noise [22]. These devices comprised an MPP backed with different cavities and the array of silencers with perforations can offer wider stopbands than the single-plate silencer.

Bloch waves were introduced to explain the wave propagation in periodic waveguides and many studies have investigated sound propagation in a spatial periodic structure. When the mufflers are distributed periodically in a duct, dispersion characteristics at certain frequencies occur where the Bloch wave cannot transmit through the structure. Bradley [23, 24] investigated the time-harmonic acoustic wave propagation in periodic waveguides both theoretically and experimentally. Sugimoto and Horioka [25] examined the dispersion characteristics of wave propagation in a tunnel with an array of Helmholtz resonators and the band structures exhibited as a result of the side branch resonance and the Bragg reflections. Wang and Mak [26] investigated the attenuation performance of a periodic Helmholtz resonator array in a duct system. Owing to the coupling of the periodic structure and the resonator, it was found that the Helmholtz resonators distributed periodically can provide much broader sound attenuation compared to a single Helmholtz resonator.

The development of the acoustic Bloch wave motivates us to combine it with the

micro-perforated tube muffler. In this paper, the Bloch wave theory is used to evaluate the sound attenuation of periodic micro-perforated mufflers. The transfer matrix of the periodic structure is derived based on the theory of wave propagation in perforated mufflers and the acoustic impedance of the micro perforation proposed by Maa [1] and the dispersion characteristics of the periodic micro-perforated mufflers are then examined. The proposed model is validated by finite element method simulation and experiments.

2. Wave propagation in a periodic array of micro-perforated tubes

2.1. Bloch waves in the periodic structure

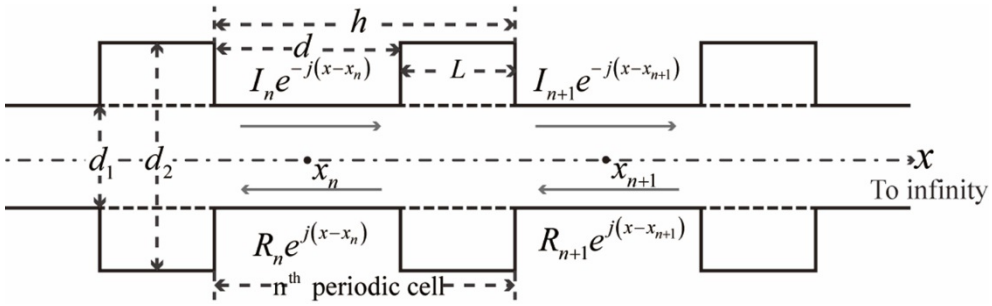

Fig. 1. A periodic array of micro-perforated mufflers.

As shown in Fig. 1, micro-perforated mufflers are distributed periodically along a circular duct. Each periodic cell here consists of a uniform duct and a micro-perforated muffler. The diameter of the inner duct of the muffler is identical

with the uniform duct. The length of the micro-perforated muffler is L and the distance between two adjacent mufflers is d. The length of a periodic cell is: $h = L+d$.

Assume that only planar waves propagate in the duct and the mufflers, the time-harmonic disturbance takes the form $\exp(-j\omega t)$. The sound wave propagating in a spatially periodic structure has been examined by Bradley [23, 24] and the solution wave functions of the periodic waveguide are Bloch wave functions which can be expressed as:

$$\begin{bmatrix} I_{n+1} \\ R_{n+1} \end{bmatrix} = \mathbf{T}\begin{bmatrix} I_n \\ R_n \end{bmatrix} = e^{-jqh}\begin{bmatrix} I_n \\ R_n \end{bmatrix} \quad \mathbf{T} = \begin{bmatrix} T_{11} & T_{12} \\ T_{21} & T_{22} \end{bmatrix} \tag{1}$$

where the transfer matrix **T** relates the sound fields at the center of the uniform duct in the n^{th} periodic cell and that in the $n+1^{th}$ periodic cell, h is the length of a periodic cell and q is called the Bloch wave number. In the n^{th} periodic cell shown in Fig. 1, the Bloch wave in the uniform duct is composed of two conventional plane waves traveling in opposite directions associated with the amplitudes I_n and R_n. In a periodic waveguide, the waves in the $(n+1)^{th}$ cell are related to ones in the n^{th} cell with e^{-jqh}. Finding the solution of the Bloch waves falls into determining the transfer matrix **T** and its eigenvalue problem:

$$\begin{bmatrix} T_{11} & T_{12} \\ T_{21} & T_{22} \end{bmatrix}\mathbf{v} = e^{-jqh}\mathbf{v} \tag{2}$$

e^{-jqh} and **v** are the eigenvalue and the corresponding eigenvector of the transfer matrix **T** of the periodic mufflers.

*2.2. The transfer matrix **T** of the periodic structure*

The sound pressure p_n and the particle velocities u_n in the n[th] periodic cell can be expressed as:

$$\begin{aligned} p_n(x) &= I_n e^{-jk(x-x_n)} + R_n e^{jk(x-x_n)} \\ \rho_0 c_0 u_n(x) &= I_n e^{-jk(x-x_n)} - R_n e^{jk(x-x_n)} \end{aligned} \tag{3}$$

where x_n is at the center of the uniform duct in the n[th] periodic cell, ρ_0 and c_0 are the ambient density and the ambient sound speed in the air.

In the n[th] periodic cell of Fig. 1, let the sound pressures and the particle velocities at the inlet ($x = x_n+d/2$) and the outlet ($x = x_{n+1}-d/2$) of the micro-perforated muffler be p_{in}, u_{in} and p_{out}, u_{out} which can be expressed with Eq. (3):

$$\begin{aligned} p_{in} &= p_n(x_n + d/2) & p_{out} &= p_{n+1}(x_{n+1} - d/2) \\ &= I_n e^{-jkd/2} + R_n e^{jkd/2} & &= I_{n+1} e^{jkd/2} + R_{n+1} e^{-jkd/2} \\ \rho_0 c_0 u_{in} &= \rho_0 c_0 u_n(x_n + d/2) & \rho_0 c_0 u_{out} &= \rho_0 c_0 u_{n+1}(x_{n+1} - d/2) \\ &= I_n e^{-jkd/2} - R_n e^{jkd/2} & &= I_{n+1} e^{jkd/2} - R_{n+1} e^{-jkd/2} \end{aligned} \tag{4}$$

The transfer matrix of sound pressures and particle velocities between the inlet and outlet of the inner duct of the micro-perforated muffler is defined as **C**. Then the sound pressure and particle velocity at the outlet of the micro-perforated muffler in the n[th] periodic cell can be expressed as.

$$\begin{bmatrix} p_{out} \\ \rho_0 c_0 u_{out} \end{bmatrix} = \mathbf{C} \begin{bmatrix} p_{in} \\ \rho_0 c_0 u_{in} \end{bmatrix} \tag{5}$$

Combining Equations (4) and (5) yields:

$$\begin{bmatrix} I_{n+1} \\ R_{n+1} \end{bmatrix} = \begin{bmatrix} 0.5e^{-jkd/2} & 0.5e^{-jkd/2} \\ 0.5e^{jkd/2} & -0.5e^{jkd/2} \end{bmatrix} \mathbf{C} \begin{bmatrix} e^{-jkd/2} & e^{jkd/2} \\ e^{-jkd/2} & -e^{jkd/2} \end{bmatrix} \begin{bmatrix} I_n \\ R_n \end{bmatrix} \tag{6}$$

According to the Eq. (1), the periodic transfer matrix **T** can be expressed as:

$$\mathbf{T}=\begin{bmatrix} T_{11} & T_{12} \\ T_{21} & T_{22} \end{bmatrix}=\begin{bmatrix} 0.5e^{-jkd/2} & 0.5e^{-jkd/2} \\ 0.5e^{jkd/2} & -0.5e^{jkd/2} \end{bmatrix}\mathbf{C}\begin{bmatrix} e^{-jkd/2} & e^{jkd/2} \\ e^{-jkd/2} & -e^{jkd/2} \end{bmatrix} \tag{7}$$

The transfer matrix **T** can be determined when the transfer matrix **C** of the micro-perforated muffler is known. In order to obtain the transfer matrix **C**, the n^{th} periodic cell is depicted in Fig. 2. The micro-perforated muffler is composed of a micro-perforated inner duct of the diameter d_1 and an outer chamber of diameter d_2. The length of the muffler is L.

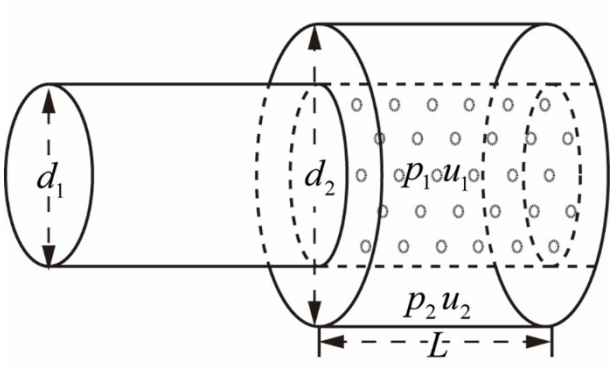

Fig. 2. The n^{th} periodic cell of the periodic micro-perforated mufflers.

Assume that only harmonic planar waves propagate in both the micro-perforated inner duct and the outer chamber (Fig. 2). In the absence of mean flow, the coupled wave equations in the inner duct and the outer chamber are expressed as follows [27]:

$$\frac{d^2 p_1}{dx^2}+\left(k^2-\frac{4}{d_1}\frac{jk}{z}\right)p_1+\left(\frac{4}{d_1}\frac{jk}{z}\right)p_2=0 \tag{8}$$

$$\frac{d^2 p_2}{dx^2}+\left(\frac{4d_1}{d_2^2-d_1^2}\frac{jk}{z}\right)p_1+\left(k^2-\frac{4d_1}{d_2^2-d_1^2}\frac{jk}{z}\right)p_2=0 \tag{9}$$

$$z=\frac{p_1-p_2}{\rho_0 c_0 u_1} \tag{10}$$

where k is the wave number, p_1 and p_2 represent the sound pressures in the inner duct and outer chamber, respectively. z is the non-dimensional acoustic impedance of the

micro perforation. According to Maa's model [6], the non-dimensional acoustic impedance z can be expressed as:

$$z = \frac{32\eta}{\sigma\rho_0 c_0}\frac{t}{d_h^2}\left[\sqrt{1+\frac{K^2}{32}}+\frac{\sqrt{2}}{32}K\frac{d_h}{t}\right]+j\frac{\omega t}{\sigma c_0}\left[1+1\Big/\sqrt{3^2+\frac{K^2}{2}}+0.85\frac{d_h}{t}\right] \quad (11)$$

where η is the viscosity of air, σ, d_h and t are the porosity (the ratio of the micro-perforated area to the area of the panel), the hole diameter and the thickness of the micro perforation, $K = d_h\sqrt{\omega\rho_0/4\eta}$.

Eq. (8) and Eq. (9) can be rewritten as:

$$\begin{bmatrix} p_1' \\ \left(\frac{dp_1}{dx}\right)' \\ p_2' \\ \left(\frac{dp_2}{dx}\right)' \end{bmatrix} = \begin{bmatrix} 0 & 1 & 0 & 0 \\ -\left(k^2-\frac{4}{d_1}\frac{jk}{z}\right) & 0 & -\frac{4}{d_1}\frac{jk}{z} & 0 \\ 0 & 0 & 0 & 1 \\ -\frac{4d_1}{d_2^2-d_1^2}\frac{jk}{z} & 0 & -\left(k^2-\frac{4d_1}{d_2^2-d_1^2}\frac{jk}{z}\right) & 0 \end{bmatrix} \begin{bmatrix} p_1 \\ \frac{dp_1}{dx} \\ p_2 \\ \frac{dp_2}{dx} \end{bmatrix} \quad (12)$$

$( )'$ denotes the derivative with respect to x. Eq. (12) can be rewritten as:

$$\begin{bmatrix} p_1' \\ \rho_0 c_0 u_1' \\ p_2' \\ \rho_0 c_0 u_2' \end{bmatrix} = \begin{bmatrix} 0 & -jk & 0 & 0 \\ -jk-\frac{4}{d_1 z} & 0 & -\frac{4}{d_1 z} & 0 \\ 0 & 0 & 0 & -j \\ \frac{4d_1}{d_2^2-d_1^2}\frac{1}{z} & 0 & -j-\frac{4d_1}{d_2^2-d_1^2}\frac{1}{z} & 0 \end{bmatrix} \begin{bmatrix} p_1 \\ \rho_0 c_0 u_1 \\ p_2 \\ \rho_0 c_0 u_2 \end{bmatrix} \quad (13)$$

$$= \mathbf{A}\begin{bmatrix} p_1 \\ \rho_0 c_0 u_1 \\ p_2 \\ \rho_0 c_0 u_2 \end{bmatrix}$$

where u_1 and u_2 are the sound particle velocities in the inner duct and outer chamber, let

$$\mathbf{A}*\mathbf{\Psi}=\mathbf{\Psi}*\mathbf{D}=\mathbf{\Psi}\begin{bmatrix}\lambda_1 & & & \\ & \lambda_2 & & \\ & & \lambda_3 & \\ & & & \lambda_4\end{bmatrix} \tag{14}$$

where λ_n is the eigenvalue of the matrix **A** and $\mathbf{\Psi}$ is the modal matrix whose columns are the eigenvectors of the matrix **A**.

Eq. (13) can be solved readily and the solution is:

$$\mathbf{\Psi}^{-1}\begin{bmatrix}p_1(x)\\ \rho_0 c_0 u_1(x)\\ p_2(x)\\ \rho_0 c_0 u_2(x)\end{bmatrix}=\begin{bmatrix}c_1 e^{\lambda_1 x}\\ c_2 e^{\lambda_2 x}\\ c_3 e^{\lambda_3 x}\\ c_4 e^{\lambda_4 x}\end{bmatrix} \tag{15}$$

where c_1, c_2, c_3 and c_4 are arbitrary constants. Then the sound pressure and particle velocity are obtained:

$$\begin{bmatrix}p_1(x)\\ \rho_0 c_0 u_1(x)\\ p_2(x)\\ \rho_0 c_0 u_2(x)\end{bmatrix}=\mathbf{\Psi}\begin{bmatrix}e^{\lambda_1 x} & & & \\ & e^{\lambda_2 x} & & \\ & & e^{\lambda_3 x} & \\ & & & e^{\lambda_4 x}\end{bmatrix}\begin{bmatrix}c_1\\ c_2\\ c_3\\ c_4\end{bmatrix}=\mathbf{\Phi}(x)\begin{bmatrix}c_1\\ c_2\\ c_3\\ c_4\end{bmatrix} \tag{16}$$

The acoustic pressures and particle velocities at the inlet and outlet of the muffler can be related by

$$\begin{bmatrix}p_1(L)\\ \rho_0 c_0 u_1(L)\\ p_2(L)\\ \rho_0 c_0 u_2(L)\end{bmatrix}=\left(\mathbf{\Phi}(0)\right)^{-1}\mathbf{\Phi}(L)\begin{bmatrix}p_1(0)\\ \rho_0 c_0 u_1(0)\\ p_2(0)\\ \rho_0 c_0 u_2(0)\end{bmatrix}=\mathbf{B}\begin{bmatrix}p_1(0)\\ \rho_0 c_0 u_1(0)\\ p_2(0)\\ \rho_0 c_0 u_2(0)\end{bmatrix} \tag{17}$$

where **B** is the transfer matrix which relates the sound pressures and particle velocities of both the inner duct and the outer chamber at the inlet and outlet of the micro-perforated muffler. Assuming that the wall of the outer chamber is rigid and the boundary condition of the outer chamber is

$$u_2(0) = 0$$
$$u_2(L) = 0 \tag{18}$$

Eq. (18) will be:

$$\begin{bmatrix} p_1(L) \\ \rho_0 c_0 u_1(L) \end{bmatrix} = \mathbf{C} \begin{bmatrix} p_1(0) \\ \rho_0 c_0 u_1(0) \end{bmatrix} = \begin{bmatrix} C_{11} & C_{12} \\ C_{21} & C_{22} \end{bmatrix} \begin{bmatrix} p_1(0) \\ \rho_0 c_0 u_1(0) \end{bmatrix} \tag{19}$$

where

$$C_{11} = B_{11} - \frac{B_{13}B_{41}}{B_{43}} \quad C_{12} = B_{12} - \frac{B_{13}B_{42}}{B_{43}}$$
$$C_{21} = B_{21} - \frac{B_{23}B_{41}}{B_{43}} \quad C_{22} = TB_{22} - \frac{B_{23}B_{42}}{B_{43}} \tag{20}$$

Equations (20) and (21) gives the transfer matrix **C** of sound pressures and particle velocities between the inlet and outlet of the inner duct of the micro-perforated muffler. The matrix relates the sound pressure and particle velocity at both ends of the muffler and now the periodic transfer matrix **T** is obtained according to Eq. (7).

2.3. Eigenvectors and eigenvalues of the periodic transfer matrix T

The transfer matrix **T** has two eigenvectors, $v_1 = \begin{bmatrix} v_{1I} & v_{1R} \end{bmatrix}^T$ and $v_2 = \begin{bmatrix} v_{2I} & v_{2R} \end{bmatrix}^T$, associated with the eigenvalues: exp(–iq_1h) and exp(–iq_2h). The eigenvectors indicate the conventional component of the Bloch waves. Take the eigenvalue v_1, for example, when the plane waves $v_{1I}e^{-jk(x-x_n)} + v_{1R}e^{jk(x-x_n)}$ propagate in the n^{th} periodic cell, the plane wave in the next cell will be $e^{-jq_1h}\left[v_{1I}e^{-jk(x-x_{n+1})} + v_{1R}e^{jk(x-x_{n+1})}\right]$. The combining of the incident and reflected wave with the ratio v_{1I}/v_{1R} or v_{2I}/v_{2R} is called the Bloch wave. The Eq. (2) can be rewritten as below:

$$\begin{bmatrix} T_{11}-e^{-jqh} & T_{12} \\ T_{21} & T_{22}-e^{-jqh} \end{bmatrix}\begin{bmatrix} v_I \\ v_R \end{bmatrix}=\begin{bmatrix} 0 \\ 0 \end{bmatrix} \tag{21}$$

Eliminating e^{-jqh}, Eq. (22) can be rewritten as:

$$T_{21}\left(\frac{v_I}{v_R}\right)^2+\left(T_{22}-T_{11}\right)\frac{v_I}{v_R}-T_{12}=0 \tag{22}$$

The ratio v_I/v_R is calculated from Eq. (23). When the ratio $\left|v_I/v_R\right|>1$, that means the magnitude of the incident wave is larger than that of the reflected wave in the periodic cell, which indicates that the total energy is transported in the direction of the propagation (+*x* direction) and this Bloch wave is categorized as a forward-going Bloch wave. For the other case, when the ratio $\left|v_I/v_R\right|<1$, the reflected wave dominates in each periodic cell and the total energy of the Bloch wave is transported in the opposite direction to the propagation (–*x* direction); this is called a backward-going Bloch wave.

As the definition of the Bloch wave in Eq. (1), the Bloch wave number *q* determines the transmission character of the Bloch waves and this can be solved by solving the characteristic equation of the eigenvalues of transfer matrix **T**:

$$\begin{vmatrix} T_{11}-e^{-jqh} & T_{12} \\ T_{21} & T_{22}-e^{-jqh} \end{vmatrix}=e^{-(qh)^2}-\left(T_{11}+T_{22}\right)e^{-jqh}+\left|\mathbf{T}\right|=0 \tag{23}$$

According to the principle of reciprocity, the determinant of the matrix **T** is unity[23]. The two solutions of Eq. (24) are q_1 and q_2 respectively. The solutions of *qh* is:

$$\cos\left(q_1h\right)=\frac{1}{2}\left(T_{11}+T_{22}\right) \tag{24}$$

This is the Bloch dispersion relation of the periodic structure. The solution of *q* is multivalued due to the inverse cosine function. *q* is real when the term on the right

side of Eq. (25) is a real number of which the absolute value is less than or equal to unity, or q is complex under other conditions. The waves in the $(n+1)^{th}$ cell are related to ones in the n^{th} cell with e^{-jqh}. When the solution of q is real, the waves traveling through a periodic cell are only changed with a phase delay. These spectral regions under this condition are known as pass bands, where waves propagate through the structure with no amplitude attenuation. In the other case when the solution of q is complex, the waves in the $(n+1)^{th}$ cell are that in n^{th} cell multiplied by $\exp(-j(q_r+jq_i)h) = \exp(-jq_rh)\exp(q_ih)$. The coefficient $\exp(q_ih)$ is necessarily less than or equal to unity according to the energy conservation theorem, otherwise the waves will become larger and larger through each periodic cell, which is not reasonable. In the spectral regions where q_ih is less than zero, the Bloch waves are attenuated by $\exp(q_ih)$ through each periodic cell. When the number of periodic cells is large enough, the waves are eliminated and cannot transmit through the whole periodic structure; such frequency regions are called stopbands.

2.4. Finite periodic micro-perforated mufflers

In the preceding sections the periodic waveguide is infinite and the downstream boundary condition is different with that in finite periodic structure. Bradley [24] also investigated the wave propagation in a semi-infinite or finite periodic waveguide. He proved that forward and backward traveling Bloch wave functions were also the solutions of the finite periodic waveguide.

For finite periodic micro-perforated mufflers with N cells, the waves in the n^{th} cell can be expressed as:

$$\begin{bmatrix} I_n \\ R_n \end{bmatrix} = \mathbf{T}\begin{bmatrix} I_{n-1} \\ R_{n-1} \end{bmatrix} = \mathbf{T}^2\begin{bmatrix} I_{n-2} \\ R_{n-2} \end{bmatrix}\cdots = \mathbf{T}^{n-1}\begin{bmatrix} I_1 \\ R_1 \end{bmatrix} \tag{25}$$

The makeup of the Bloch waves is determined by the boundary conditions at the beginning and end of the periodic duct.

For a finite periodic array of n micro-perforated mufflers, the waves in the first cell can be expressed as the linear superposition of the two types of Bloch wave:

$$\begin{bmatrix} I_1 \\ R_1 \end{bmatrix} = a\begin{bmatrix} v_{1I} \\ v_{1R} \end{bmatrix} + b\begin{bmatrix} v_{2I} \\ v_{2R} \end{bmatrix} \tag{26}$$

where a and b are arbitrary constants and can be solved with the boundary conditions.

The waves in the n^{th} cell are:

$$\begin{aligned} \begin{bmatrix} I_n \\ R_n \end{bmatrix} &= \mathbf{T}^{n-1}a\begin{bmatrix} v_{1I} \\ v_{1R} \end{bmatrix} + \mathbf{T}^{n-1}b\begin{bmatrix} v_{2I} \\ v_{2R} \end{bmatrix} \\ &= e^{-jq_1h(n-1)}a\begin{bmatrix} v_{1I} \\ v_{1R} \end{bmatrix} + e^{-jq_2h(n-1)}b\begin{bmatrix} v_{2I} \\ v_{2R} \end{bmatrix} \end{aligned} \tag{27}$$

If the finite periodic micro-perforated mufflers end with anechoic termination, the incident wave in the first cell is I_1 and the transmitted wave in the last cell is I_n. The transmission loss of the n micro-perforated mufflers can be calculated as:

$$TL = 20\log_{10}\left|\frac{I_1}{I_n}\right| = 20\log_{10}\left|\frac{av_{1I} + bv_{2I}}{e^{-jq_1d(n-1)}av_{1I} + e^{-jq_2d(n-1)}bv_{2I}}\right| \tag{28}$$

Anechoic termination means that there is no reflection in the last cell:

$$R_n = e^{-jq_1h(n-1)}av_{1R} + e^{-jq_2h(n-1)}bv_{2R} = 0 \tag{29}$$

therefore

$$\frac{b}{a} = -\frac{e^{-jq_1h(n-1)}v_{1R}}{e^{-jq_2h(n-1)}v_{2R}} \tag{30}$$

Substituting Eq. (31) for Eq. (29), the transmission loss of the finite periodic micro-perforated mufflers is obtained.

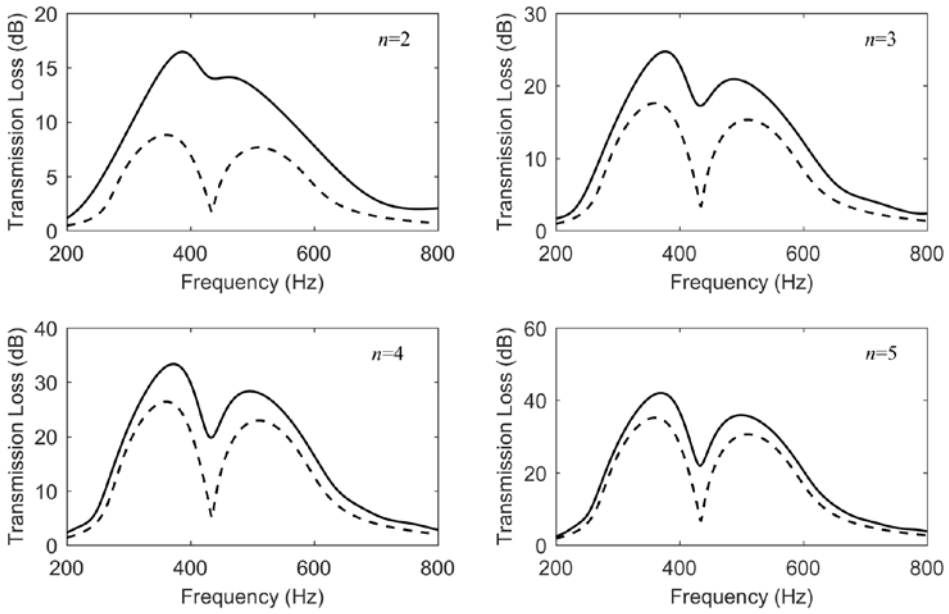

Fig. 3. The comparison of transmission loss of *N* finite periodic expansion chamber mufflers (solid lines) and *N* mufflers of an infinite periodic expansion chamber mufflers (dash lines).

In an infinite periodic waveguide as shown in Figure 1, only the forward-traveling Bloch waves propagate and the TL of *n* mufflers of the infinite periodic waveguide can be readily calculated as $TL_{\inf} = 20\log_{10}\left|av_{1I}/\left(e^{-jqhn}av_{1I}\right)\right|$. Fig.3 shows the comparison of the TL of the *n* finite periodic micro-perforation mufflers and that of the infinite periodic micro-perforation mufflers. The dimensions of the mufflers were the same as shown in Table 1 and the periodic distance *h* was 0.40 m. As the number of the finite periodic muffler increases, the TL of *n* finite periodic micro-perforation mufflers is approaching to that in the infinite periodic waveguide. The stopbands and passbands of

the finite expansion mufflers are similar to that in an infinite system. Therefore, the stopbands and passbands determined with Bloch wave theory under the infinite periodic assumption can be used in the finite periodic micro-perforation mufflers to predict its attenuation performance.

3. Simulation and experiment

3.1. FEM simulation

As the periodic structure in this study is structurally symmetric around the axis, a 2D axisymmetric finite element method (FEM) was used to verify the one dimensional theoretical analysis of the finite micro-perforated mufflers in the previous sections and then is also verified itself by experimental results in the next section.

The wave propagation is governed by the Helmholtz Equation in the inner duct and the outer chamber of the muffler. The numerical model is composed of a circular duct with three micro-perforated mufflers. The sound source is located at the beginning of the duct and modeled with the plane wave radiation boundary condition with amplitude $p_0 = 1$ which is the incident wave to the periodic micro-perforated mufflers. The anechoic termination of the main duct is modeled with a non-reflective boundary condition and a probe at the termination boundary is used to measure the transmitted wave pressure. Therefore, the transmission loss of the finite periodic

micro-perforated muffler can be easily obtained with the transmitted pressure at the termination boundary and the incident wave pressure.

In the simulation, the temperature and the pressure in air are 20 degrees Celsius and 1 atmosphere respectively. The micro-perforation was not simulated directly. Instead, the micro-perforation is modeled by the interior impedance boundary condition. The interior impedance relates the acoustic pressures in the inner duct and the muffler chamber through the boundary. Here the impedance of the micro-perforation is defined according to Maa's model as Eq. (11). Table 1 gives the dimensions of the finite periodic micro-perforated muffler.

3.2. Experimental Studies

The configuration of the experimental setup is shown in Fig. 4. The dimensions of the mufflers were the same as shown in Table 1 and the periodic distance *h* was 0.40 m. The testing apparatus consists of four Brüel & Kjær microphones Type 4935, Brüel & Kjær LAN-XI acquisition hardware Type 3160-B-042, and Brüel & Kjær power amplifier Type 2706. The duct walls were acrylic 3 mm thick.

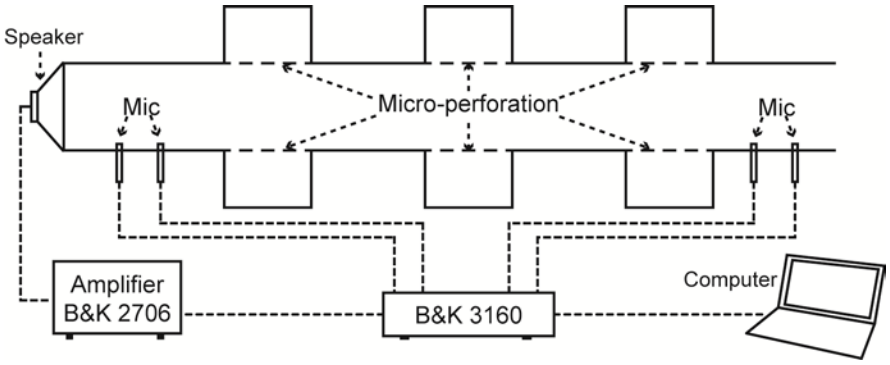

Fig. 4. The experimental setup.

In order to measure accurately the transmission loss of the periodic structure, the two-load method was applied in the experiment to measure the transfer matrix of the apparatus under test [28]. The two-load method means that the experiment was carried out with two different duct terminations (one is rigid end termination and one is a termination with absorptive materials) and then the transfer matrix of the structure could be calculated by the measured sound pressure levels under the two different termination conditions. Once the matrix of the finite periodic micro-perforated muffler is measured, then the transmission loss of the muffler can be calculated based on the transfer matrix.

Fig. 5 shows the comparison of the transmission loss between the theory, the FEM simulation and the experiments for a periodic array of three micro-perforated mufflers. It can be seen that the experimental results agree well with the theoretical results and the FEM simulation. The transmission loss predicted by the theoretical model agrees well with the simulation result obtained using the FEM method for the three micro-perforated mufflers. Here the differences between the FEM and the theoretical model is very small, this is reasonable because both the FEM and the

theoretical model use the Maa's impedance model to simulate the micro-perforation and assume only plane waves propagating in the ducts.

The difference in magnitude between the experiment and the theoretical study is mainly due to the discrepancies between the one dimensional theoretical model and the three dimensional experiment. It is assumed in the theoretical model and the FEM that only plane waves propagate in the inner duct and the outer chamber. However, the higher order modes below the cut-off frequencies are evanescent and cannot decay sufficiently if the muffler is not long enough. These higher order modes are different from the plane wave assumption of the theory and FEM. In addition, it is a fact that the acoustic impedance of the micro-perforation used in previous studies is a simplified model and does not consider the hole interactions (when the orifices of the micro-perforation are located closely. The interaction effect between adjacent orifices cannot be neglected and influence the acoustic performance of the micro-perforation muffler) that also contribute to the differences between the experiment and the theory.

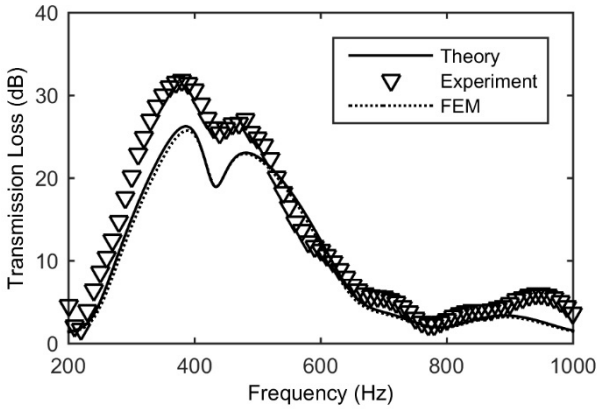

Fig. 5. A comparison of transmission loss of the three periodic micro-perforated mufflers between theory, FEM simulation and experiment result.

4. Discussion

4.1. Comparison of transmission loss with the dissipative muffler

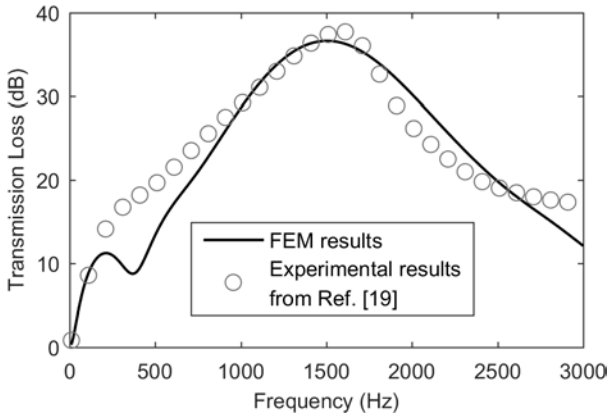

Fig. 6. The comparison of the transmission loss between the MPP muffler and the dissipative muffler.

Fig. 6 provides a comparison of the transmission loss between the MPP muffler and the dissipative muffler (a muffler filled with fibrous material). The solid line represents the FEM simulation result of the single MPP muffler and the circles represent the experiment result of a dissipative muffler from reference [19]. The dimensions of the MPP muffler are the same as the dissipative muffler. The hole diameter, the thickness and the porosity of the micro-perforation are set as 0.1 mm, 3 mm and 0.25, respectively. It can be seen from Fig. 5 that with the same muffler size, the MPP muffler can provide a similar attenuation performance with the traditional dissipative muffler.

4.2. Comparison of transmission loss with the regular MPP muffler

The sound attenuation performance of the periodic MPP muffler is first compared with a single MPP muffler by FEM method. The geometries of the MPP muffler are shown in Table 1. The multiple MPP mufflers are composed of three equally spaced MPP mufflers.

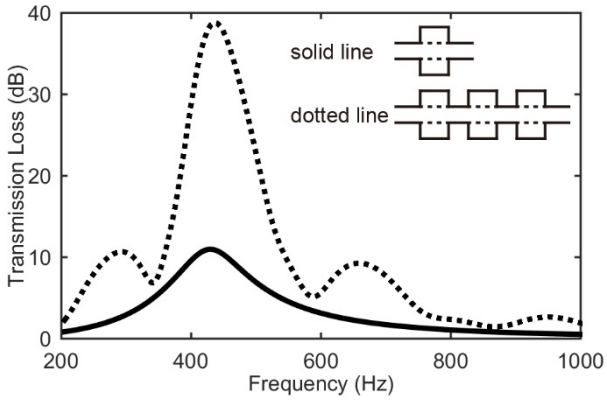

Fig. 7. Transmission loss of a duct with a single MPP muffler (solid line) and the three periodic MPP mufflers (dotted line).

As shown in Fig. 7, the solid line is the transmission loss of a single MPP muffler and the dotted line is that of three periodic MPP mufflers with a distance 0.46 m between the mufflers. It is obvious that the periodic MPP mufflers outperform the single MPP muffler in terms of the peak transmission loss and the effective frequency range. However, the volume and the length of the periodic muffler is much larger than the single MPP muffler. In order to investigate the cost resulting from such repetitive units, three MPP mufflers in series (connected with no distance) are chosen for comparison so that the volume of the mufflers in the two cases are the same and the

only difference is the distance between mufflers. Fig. 8 shows a comparison of the transmission loss between the reference mufflers and the three periodic micro-perforated mufflers with 0.46 m between each other. In the FEM simulation, the distance between mufflers *d* is set as 0 and 0.46 m respectively.

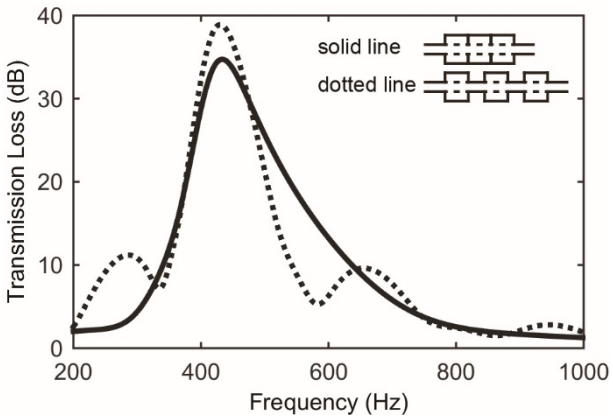

Fig. 8. Transmission loss of a duct with three periodic micro-perforated mufflers. The distance *d* between two mufflers is set at 0 (solid line) and 0.46 m (dotted line).

As seen in Fig. 8, the transmission loss of the directly connected mufflers (solid line) reaches maximum at 430 Hz which is the resonant frequency. When d = 0.46 m (periodic distance h = 0.56 m), compared to the directly connected MPP mufflers, the maximum transmission loss of the three periodic MPP mufflers is increased at the resonant frequency but the effective attenuation frequency range is narrowed. Furthermore, two stopbands occur at around 300 Hz and 640 Hz. In this case, the performance of the periodic MPP mufflers outperform the directly connected MPP mufflers around the resonance frequency and the first stopband.

4.3. The effect of the periodic distance

The stopbands of the periodic MPP mufflers occur as a result of the coupling between the resonance of the muffler itself and the Bragg reflection in the periodic structure [23]. For a periodic cell of length *h*, the Bragg stopbands occur around the Bragg frequency: $f_B = nc/2h$ $(n = 1, 2, \cdots)$. For the case in Fig. 8, the periodic distance h = 0.56 m and the first two Bragg frequency are 306 Hz and 612 Hz.

In order to investigate the coupling of the Bragg reflection and the resonance of the micro-perforated mufflers, Fig. 8 shows the imaginary part of *qh* of this case. As analyzed in section 2, the frequencies in Fig. 9, where an imaginary part of *qh* is less than zero, means that the Bloch waves are attenuated by exp(Im(*qh*)) and these spectral regions are referred as stopbands. The stopband II is mainly due to the resonance of the micro-perforated mufflers and the stopbands I and III are mainly due to the periodic structure.

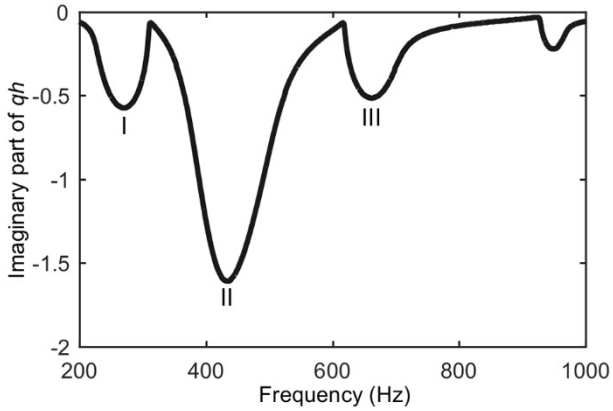

Fig. 9. Imaginary part of *qh*.

Eq. (25) reveals the dispersion characteristic of the periodic micro-perforated muffler. The imaginary part of *qh* is determined by the periodic cell matrix as a result of the coupling the micro-perforated muffler and the periodic structure. Bragg resonance is a result of cumulative reflection from each unit of the periodic structure. Since the Bragg resonance can narrow the effective noise control frequency range as shown in Fig. 8, it may influence the performance of the muffler in another way, by adjusting the periodic distance.

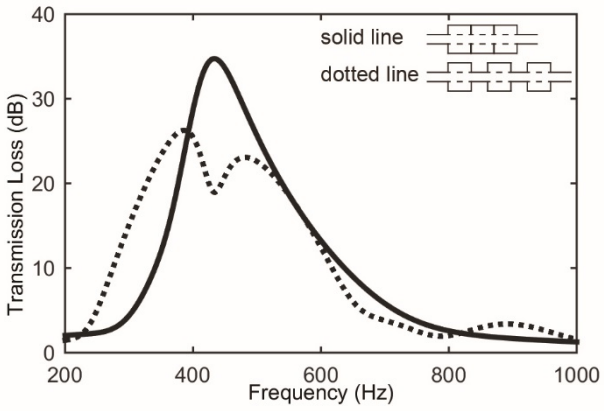

Fig. 10. Transmission loss of a duct with three periodic micro-perforated mufflers. The distance between two mufflers is set at 0 (solid line) and 0.3 m (dotted line).

In Fig. 10 the distance between two mufflers *d* is set as 0.30 m and the corresponding periodic distance *h* is 0.40 m. The first two Bragg frequencies are 429 Hz and 860 Hz. In this case, although the peak of the transmission loss is decreased compared to that of the directly connected mufflers, the transmission loss is increased at lower frequencies and the efficient frequency range is widened, which has potential

implications for lower frequency noise control.

A periodic array of three micro-perforated mufflers can provide more than 15 dB noise attenuation from 300 Hz to 580 Hz. The results verify that, with appropriate periodic distance, micro-perforated mufflers can attenuate noise over a wider frequency range compared to directly connected mufflers. It can also be noted from Fig. 9 that there is a trough at around 430 Hz. This occurs due to the interaction between the Bragg reflection and the resonance of the micro-perforated tube. At the cost of such a trough, the effective noise control frequency range is extended and shifted to a lower frequency range.

The above predicted transmission loss at a different periodic distance demonstrates that the Bragg resonance has a manipulation effect on the transmission loss of the micro-perforated muffler. The transmission loss of the periodic micro-perforation mufflers is determined by the stopbands (around resonant frequency) caused by the micro-perforation muffler and the stopbands (around Bragg frequencies) caused by the periodic structure. Compared to directly connected MPP mufflers, the insertion of uniform duct mainly influences the transmission loss around the Bragg frequencies. Therefore, if we want to change the transmission loss at certain frequency, the periodic distance can be chosen that the certain frequency is one of the brag frequencies of the periodic structure. On this basis, an appropriate periodic distance can be achieved with trial and error which can contribute to the control of lower frequency noise within a broader frequency range and achieve higher transmission loss around the resonant frequency.

5. Conclusions

This paper presents a detailed examination of the acoustic attenuation of a periodic array of micro-perforated tube mufflers. Owing to its sub-millimeter perforation, the micro-perforated muffler can provide considerable sound attenuation for duct noise without using absorptive materials. When such mufflers are located periodically in a duct, the periodic structure produces dispersion characteristics in the overall transmission loss.

The periodic distance of the periodic micro-perforation mufflers has an important effect on the overall sound attenuation performance. When the mufflers are periodically spaced, the Bragg resonance resulting from the periodic structure has a modulation effect on the transmission loss of the periodic micro-perforated mufflers. The transmission loss will be changed around the Bragg frequencies. By selecting an appropriate periodic distance, the periodic structure can influence the sound attenuation performance: the control of lower frequency noise within a broader frequency range or achieve higher transmission loss around the resonant frequency. Such a periodic structure provides a way of modifying the transmission loss of the micro-perforated muffler by inserting uniform ducts between mufflers provided that the space is not limited and has a potential application in muffler design.

REFERENCES

[1] D. Y. Maa. Theory and design of microperforated panel sound-absorbing constructions. SCIENCE CHINA Mathematics 1975; 18: 55-71.

[2] C. Wang, L. Cheng, J. Pan, and G. Yu. Sound absorption of a micro-perforated panel backed by an irregular-shaped cavity. J Acoust Soc Am 2010; 127: 238-246.

[3] P. Cobo, J. Pfretzschner, M. Cuesta, and D. K. Anthony. Hybrid passive–active absorption using microperforated panels. J Acoust Soc Am 2004; 116: 2118-2125.

[4] T. Bravo, C. Maury, and C. Pinhède. Vibroacoustic properties of thin micro-perforated panel absorbers. J Acoust Soc Am 2012; 132: 789-798.

[5] C. N. Wang. Numerical decoupling analysis of a resonator with absorbent material. Appl Acoust 1999; 58: 109-122.

[6] D. Y. Maa. Potential of microperforated panel absorber. J Acoust Soc Am 1998; 104: 2861-2866.

[7] H. V. Fuchs and X. Zha. Micro-perforated structures as sound absorbers - a review and outlook. Acta Acust United Ac 2006; 92: 139-146.

[8] F. Asdrubali and G. Pispola. Properties of transparent sound-absorbing panels for use in noise barriers. J Acoust Soc Am 2007; 121: 214-221.

[9] J. Kang and M. W. Brocklesby. Feasibility of applying micro-perforated absorbers in acoustic window systems. Appl Acoust 2005; 66: 669-689.

[10] C. Wang and L. Huang. On the acoustic properties of parallel arrangement of multiple micro-perforated panel absorbers with different cavity depths. J Acoust Soc

Am 2011; 130: 208-218.

[11] C. Wang, L. Huang, and Y. Zhang. Oblique incidence sound absorption of parallel arrangement of multiple micro-perforated panel absorbers in a periodic pattern. J Sound Vib 2014; 333: 6828-6842.

[12] M. Q. Wu. Micro-perforated panels for duct silencing. Noise Control Eng J 1997; 45: 69-77.

[13] L. Xiang, S. Zuo, M. Zhang, J. Hu, and G. Long. Study of micro-perforated tube mufflers with adjustable transmission loss. J Acoust Soc Am 2013; 134: 4217-4217.

[14] D. Herrin, J. Liu, and A. Seybert. Properties and applications of microperforated panels. Sound and Vibration 2011; 45: 6.

[15] J. Liu, D. W. Herrin, and A. F. Seybert. Application of micro-perforated panels to attenuate noise in a duct. SAE Technical Paper 2007; 2007-01-2196.

[16] S. Allam and M. Åbom. A new type of muffler based on microperforated tubes. J Vib Acoust 2011; 133: 031005-031005-8.

[17] R. Kabral, H. Rämmal, and J. Lavrentjev. Acoustic studies of micro-perforates for small engine silencers. SAE Technical Paper 2012; 2012-32-0107.

[18] A. Selamet, I. Lee, Z. Ji, and N. Huff. Acoustic attenuation performance of perforated absorbing silencers. SAE Technical Paper 2001; 2001-01-1435.

[19] A. Selamet, M. B. Xu, I. J. Lee, and N. T. Huff. Analytical approach for sound attenuation in perforated dissipative silencers. J Acoust Soc Am 2004; 115: 2091-2099.

[20] J. W. Sullivan and M. J. Crocker. Analysis of concentric‐tube resonators having

unpartitioned cavities. J Acoust Soc Am 1978; 64: 207-215.

[21] X. N. Wang, Y. S. Choy, and L. Cheng. Hybrid noise control in a duct using a light micro-perforated plate. J Acoust Soc Am 2012; 132: 3778-3787.

[22] Y. Liu, Y. S. Choy, and Y. K. Chiang, Performance of multiple micro-perforated panels in a duct, *Proceedings of Internoise 2014*, Melbourne, Australia, 2014.

[23] C. E. Bradley. Time harmonic acoustic Bloch wave propagation in periodic waveguides. Part I. Theory. J Acoust Soc Am 1994; 96: 1844-1853.

[24] C. E. Bradley. Time harmonic acoustic Bloch wave propagation in periodic waveguides. Part II. Experiment. J Acoust Soc Am 1994; 96: 1854-1862.

[25] N. Sugimoto and T. Horioka. Dispersion characteristics of sound waves in a tunnel with an array of Helmholtz resonators. J Acoust Soc Am 1995; 97: 1446-1459.

[26] X. Wang and C. M. Mak. Wave propagation in a duct with a periodic Helmholtz resonators array. J Acoust Soc Am 2012; 131: 1172-1182.

[27] A. Selamet, I. J. Lee, and N. T. Huff. Acoustic attenuation of hybrid silencers. J Sound Vib 2003; 262: 509-527.

[28] ASTM E2611-09 Standard test method for measurement of normal incidence sound transmission of acoustical materials based on the transfer matrix method (American Society for Testing and Materials, Philadelphia, 2009)

Table 1. The configuration of the micro-perforated muffler

Property	**Value**
The inner diameter	d_1 = 94 mm
The outer diameter	d_2 = 154 mm
The length of the micro-perforated tube	L = 100 mm
The hole diameter of the micro perforation	d_h = 1 mm
The thickness of the micro perforation	t = 3 mm
The porosity of the micro perforation	σ = 0.0085
Temperature	20 ℃
Pressure	1 atm
Viscosity in air	$1.8 \cdot 10^{-5}$ Pa·s

Figure captions

Fig. 1. A periodic array of micro-perforated mufflers.

Fig. 2. The n^{th} periodic cell of the periodic micro-perforated mufflers

Fig. 3. The comparison of transmission loss of N finite periodic expansion chamber mufflers (solid lines) and N mufflers of an infinite periodic expansion chamber mufflers (dash lines).

Fig. 4. The experimental setup.

Fig. 5. A comparison of transmission loss of the three periodic micro-perforated mufflers between theory, FEM simulation and experiment result.

Fig. 6. The comparison of the transmission loss between the MPP muffler and the dissipative muffler.

Fig. 7. Transmission loss of a duct with a single MPP muffler (solid line) and the three periodic MPP mufflers (dotted line).

Fig. 8. Transmission loss of a duct with three periodic micro-perforated mufflers. The distance d between two mufflers is set at 0 (solid line) and 0.46 m (dotted line).

Fig. 9. Imaginary part of *qh*.

Fig. 10. Transmission loss of a duct with three periodic micro-perforated mufflers. The distance between two mufflers is set at 0 (solid line) and 0.3 m (dotted line).